Soft Matter

PAPER

View Article Online
View Journal | View Issue

Cite this: *Soft Matter*, 2025, **21**, 3829

Corrosion-resistant omniphobic coating for low-carbon steel substrates using silica layers enhanced with ethylenediamine tetraacedic acid

Parnian Mirabi, [a] Fariba Vaez Ghasemi, [b] Masoud Zakeri, [c] Ibrahim Ogunsanya [c] and Kevin Golovin *[ab]

The present work develops a highly liquid repellent, *i.e.* omniphobic, coating designed specifically for metallic substrates like low carbon steels and evaluates its potential as a barrier to corrosion. Polydimethylsiloxane (PDMS) chains are grafted to an intermediary silica layer *via* the hydrolysis and polycondensation of a difunctional chlorosilane monomer, resulting in a contact angle hysteresis of ~3° when deposited on unpolished low carbon steel substrates. However, the use of chlorosilanes to fabricate the omniphobic PDMS can corrode steel. To circumvent this, the coating uses a phosphate buffer solution to partially neutralize the silica precursor solution, and ethylenediamine tetraacedic acid (EDTA) to passivate any released Fe ions. The inhibition of corrosion is evidenced visually and by unchanging surface metrology parameters even after two months following coating deposition. Potentiodynamic polarization data indicate that the omniphobic layer provides a barrier to water ingress, as evidenced by a current density of ~10^{-6} A cm^{-2}, two orders of magnitude lower than the steel coated with the silica but without the PDMS chains. Electrochemical impedance spectroscopy data indicates the absence of an inductive loop (*i.e.* no ongoing corrosion) and a high polarization resistance of 40 000 Ω cm^2 for the omniphobic coating. This work not only indicates that omniphobic grafted polymer chains like PDMS exhibit anti-corrosion properties, but also provides a method for depositing such coatings onto metals without corroding the substrate, even when using chlorosilane precursors that evolve hydrochloric acid.

Received 13th January 2025,
Accepted 7th April 2025

DOI: 10.1039/d5sm00046g

rsc.li/soft-matter-journal

Introduction

In recent years, the development of surfaces that can repel a wide range of high- and low-surface tension liquids, *i.e.*, omniphobic surfaces, has drawn significant attention due to their diverse applications in medical devices,[1–3] self-cleaning coatings,[4] wastewater treatment,[5,6] and paper products.[7] One promising class of omniphobic surface is liquidlike grafted polymer chains, typically polydimethylsiloxane (PDMS) or perfluoropolyether (PFPE), where single polymer chains well-above their glass transition temperature are covalently tethered to the surface from one end only, leaving the remainder of the chain to freely flex, rotate, and even exhibit flow-like properties.[8] The typical route for synthesizing liquidlike polymer brushes involves the acid-catalyzed hydrolysis and subsequent polycondensation of either chlorosilanes[9] or alkoxysilanes,[10] using glass or Si wafers as a substrate. However, these synthesis routes cannot be readily applied to metallic substrates like steel, due to the risk of corrosion from the HCl generated during the hydrolysis of chlorosilanes, or the acid used to catalyze alkoxysilane hydrolysis. Accordingly, not only are current deposition strategies not amenable to metallic surfaces, but any potential anti-corrosion properties of such omniphobic surfaces remain largely unexplored. The purpose of this study was to develop a non-corroding method for grafting liquidlike PDMS on low-carbon steel, and to assess the anti-corrosion performance of such an omniphobic surface.

Omniphobic surfaces may be characterized by their low contact angle hysteresis (CAH) with various liquids, defined as the difference between the advancing (θ_A) and receding (θ_R) contact angles of droplets, or CAH = $\theta_A - \theta_R$. For example, whereas common engineering surfaces exhibit CAH > 20° for most fluids, CAH ~ 0° has been reported on liquidlike grafted PDMS by several groups.[10–13] The zero or near zero CAH of omniphobic PDMS surfaces has been attributed to the mobile state of the polymer chains, as well as the almost perfectly

[a] *Department of Materials Science and Engineering, Toronto, ON, Canada. E-mail: Kevin.golovin@utoronto.ca*
[b] *Department of Mechanical & Industrial Engineering, Toronto, ON, Canada*
[c] *Department of Civil & Mineral Engineering University of Toronto, Toronto, ON, Canada*

smooth nature of the coating.[8,10] However, with a total coating thickness < 10 nm, the grafted layer is quite conformal and the surface will only be smooth if the underlying substrate is also atomically flat. For float glass and single crystals of silicon this is achievable on an industrial scale, but even highly polished steel typically exhibits roughness on the order of 10 s of nanometers, and as-cast or as-drawn steel is typically rough on the micron scale.[14]

To circumvent this issue, Khatir *et al.*[9] pioneered a substrate-independent approach to achieve low CAH with grafted PDMS chains even on rough surfaces. Their method involves first depositing a thin, smooth silica layer, which covers the inherent roughness of the underlying substrate, as well as provides reactive silanol groups to which the PDMS chains may be anchored. This technique has been successfully adapted to many substrates, such as textiles, paper, glass, and plastics, to name a few. Moreover, the deposition of these omniphobic coatings can be scaled to large surface areas through spray-coating or conventional painting techniques. Nonetheless, there is a limitation when applying this method to metallic surfaces. The silica layer is formed using acid-catalyzed hydrolysis of alkoxysilanes, again creating the risk of corrosion for metallic substrates (Fig. 1). Methods are still needed to eliminate the corrosion associated with producing omniphobic surfaces in this manner.

Various techniques have been developed to improve the corrosion resistance of metals. These include methods such as conversion coatings,[15–18] cathodic protection,[19–22] organic coatings,[23–25] nanocomposites,[26–28] and the use of chelating agents as corrosion inhibitors.[29–31] Chelating agents are most amenable to the deposition of the silica layer discussed above because they can be integrated into an existing surface coating, unlike techniques that require additional non-omniphobic coatings or layers. Moreover, chelating agents, by nature, bind with metal ions, providing a direct and efficient protection mechanism. Ethylenediamine tetraacetic acid (EDTA) is a leading chelating agent that possesses six available binding sites for metal ions.[32,33] Such a hexadentate ligand forms a cage-like complex preventing metallic ions from further interactions with their corrosive environment. This behavior parallels that of amino acids, forming double zwitterionic structures in solution.[34] Therefore, adopting chelating agents like EDTA is a practical and effective strategy for enhancing corrosion resistance.

This work presents the development of an omniphobic coating specifically designed for metallic surfaces, which does not corrode the substrate. To achieve this, EDTA is incorporated as a chelating agent within the silica sol–gel formulation, along with a pH alternation procedure to partially neutralize the solution prior to deposition. Using these two strategies, PDMS chains grown using chlorosilanes do not corrode the underlying carbon steel surfaces, allowing for the omniphobic properties to be retained long term. Moreover, the anti-corrosion properties of the coating are studied *via* potentiodynamic polarization and electrochemical impedance spectroscopy (EIS), highlighting the efficacy of omniphobic, grafted PDMS chains as corrosion-inhibiting layers.

Experimental

Materials

Toluene (99.5%), isopropyl alcohol (99%), ethanol (90%), Sodium Hydroxide pellets (reagent grade), and 12 M hydrochloric acid were purchased from VWR. Tetraethoxysilane

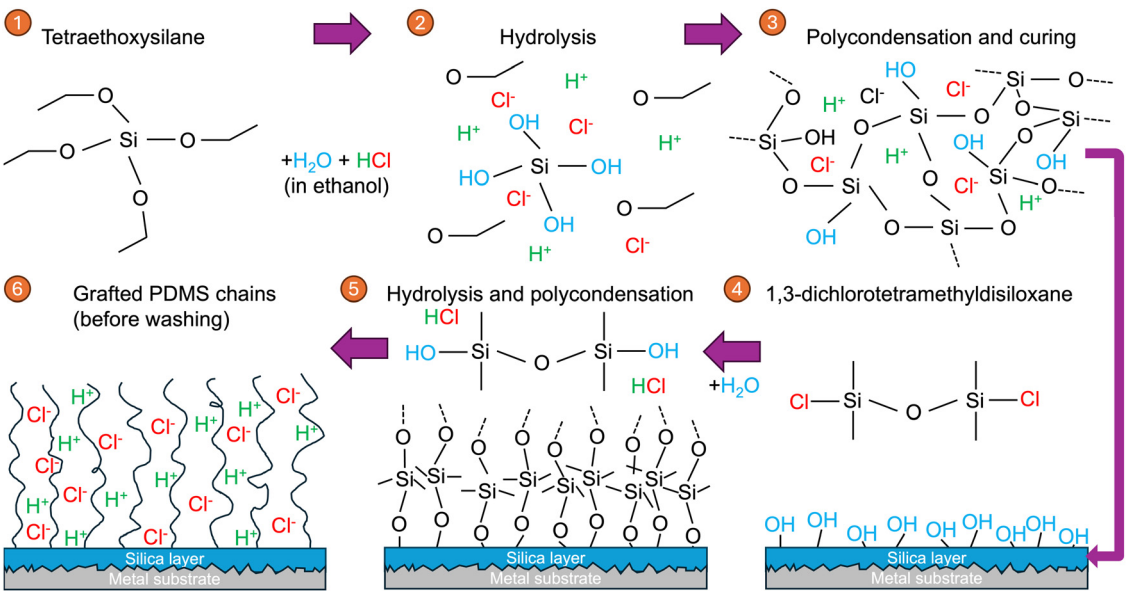

Fig. 1 Typical route of silica layer deposition (steps 1–3) and omniphobic PDMS grafting to the silica layer using chlorosilanes (steps 4–6). Chlorides are present throughout both processes. Note the schematics are not to scale, and typically the silica layer is ~300 nm thick,[9] whereas the omniphobic PDMS is around 4 nm thick.[8]

(TEOS, 98%) was purchased from Alfa Aesar. 1,3-Dichlorotetramethyldisiloxane (97%) was purchased from Gelest. Low carbon steel sheets were purchased from Metal Supermarkets. The mild steel was cold rolled with a composition <0.15 C, <0.60 Mn, <0.035 P, and <0.04 S per the manufacturer specifications. Sodium borate decahydrate (99.5%) and ethylenediaminetetraacetic acid tetrasodium (EDTA, ultra-pure grade) salt were purchased from Sigma Aldrich. Phosphate buffer solution (0.1 M) was purchased from Ward's Science.

Methods

Coating preparation. A thin silica layer on substrates was fabricated using the sol–gel technique and tetraethoxysilane (TEOS) as the silica alkoxide in an acid-catalyzed process, as described previously.[9] Briefly, a mixture was prepared consisting of TEOS : ethanol : water : HCl in a molar ratio of 1 : 3.8 : 6.4 : 0.085. The procedure began by stirring ethanol and TEOS at 500 rpm at ambient temperature for 1 minute. Subsequently, water and HCl were incorporated, and the temperature was raised to 60 °C. This solution was then stirred continuously for 3 hours before being allowed to cool to room temperature. The solution was then allowed to age for 3 days at room temperature.

In a separate preparation, a 0.1 M EDTA solution was formulated using a 0.1 M phosphate buffer at a pH of 6.5. This EDTA solution was then combined with the aged silica solution in a 1 : 1 ratio and stirred at 500 rpm for 5 minutes at room temperature.

To coat the low carbon steel substrates they were dip-coated in the silica or silica/EDTA solutions using an Ossila automated dip-coater at an immersion rate of 300 mm min^{-1} and a withdrawal rate of 20 mm min^{-1}. Prior to dip coating the substrates were cleaned with isopropyl alcohol. After dip-coating, the substrates were cured in an oven at 110 °C for 10 minutes.

PDMS brush deposition. The silica or silica/EDTA coated metal samples were placed in 60 × 60 mm Petri dishes with 150 μL of 1,3-dichlorotetramethyldisiloxane held in a small vial. The Petri dish was then closed for 8 min to allow for the grafting of the PDMS chains *via* hydrolysis and polycondensation. Following this, the substrates were removed from the Petri dish and were washed with toluene and isopropyl alcohol to remove any non-bonded PDMS chains.

Characterization techniques

Surface characteristics. Advancing and receding contact angles were measured with water using a Ramé-Hart 260 Contact Angle Goniometer, employing the sessile droplet method. Contact angles were measured by either slowly introducing or gradually extracting liquid from ~10 μL droplets gently deposited on the sample surfaces. The onset of contact line movement was used to establish when to measure the angles. Measurements were taken at three distinct positions on each sample, and the mean value is reported.

A 3D scanning laser microscope (Olympus LEXT OLS5000) was used to measure root-mean-squared surface roughness (S_q) and valley depth (S_v) using a 20× magnification lens. The same microscope was also used for optical imaging of the surfaces, using a 100× lens. Coating thickness was also analyzed using the same 100× lens, with an additional 8× zoom applied. Each surface was imaged at three random locations and what is reported in the manuscript are the mean and standard deviation of the three measurements. As is standard practice with the Olympus LEXT OLS5100 3D laser scanning microscope, imaging noise was removed from the optical scans using a 'nearest neighbor' algorithm where the height at each measurement point was averaged with the surrounding eight points.

Surface morphology was examined using a Thermo Scientific Quattro environmental scanning electron microscope (ESEM). SEM imaging, combined with elemental analysis through energy dispersive X-ray spectroscopy (EDS), was performed at an accelerating voltage of 10 kV to achieve high resolution and sufficient penetration depth for precise material characterization.

Electrochemical characterization. A three-electrode electrochemical cell setup was employed, comprising of: (i) a bare carbon steel (as reference for comparison) or coated carbon steel as the working electrode, (ii) a saturated calomel electrode (SCE) functioning as the reference electrode, and (iii) a platinum mesh acting as the counter electrode. These electrodes were exposed to 0.1 M borate buffer solution (pH 6) for testing.

Four electrochemical tests were employed in series. The open circuit potential (OCP) of the steel sample was recorded for a duration of 30 minutes to ensure that the samples stabilized in their solution environment. Subsequently, potentiodynamic linear polarization resistance (LPR) test, using potential values ranging from −10 mV to +10 mV with respect to OCP using a scan rate of 0.167 mV s^{-1} per ASTM G59 standard, was performed using Parstat 2263. Electrochemical impedance spectroscopy (EIS) measurements were performed using Gamry Reference 600 by scanning from a frequency range of 100 000 Hz to 0.1 mHz within a potential window of −10 mV to +10 mV relative to OCP. Afterwards, a potentiodynamic nonlinear polarization measurement was performed by scanning from −0.85 V (relative to SCE) to +0.3 V (relative to OCP) using a scan rate of 0.167 mV s^{-1} per the ASTM G59 standard.

Results and discussion

Upon immersing and removing the steel substrate into the silica precursor solution that did not contain EDTA, immediate corrosion was visually observed, revealed by a noticeable color alteration on the surface (Fig. 2(a)). Over 10 days, a rust layer was visually apparent on the silica-coated sample, depicted schematically in Fig. 2(c). This rapid corrosion can be attributed to the acidity of the solution, which contained HCl, and was measured to have a pH of approximately 1.5. To mitigate this, the pH of the solution was adjusted to 5.5 using a 0.1 M solution of NaOH immediately preceding the dip coating process. A pH of 5.5 was found to be the highest value that would still give a ~30 min window to deposit the coating

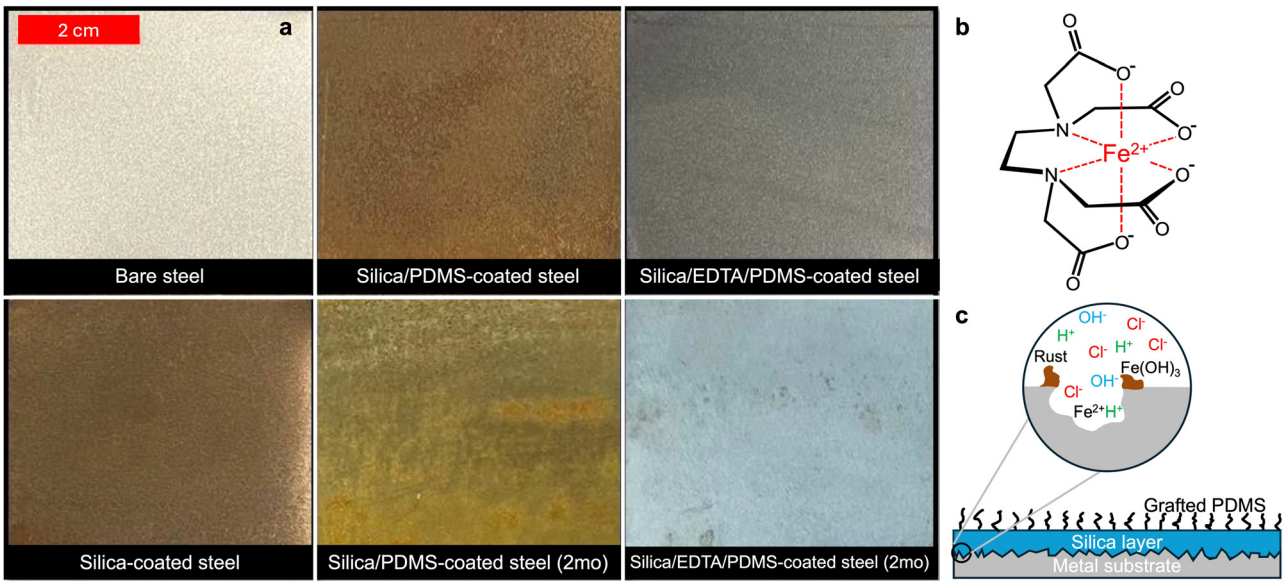

Fig. 2 (a) Optical images of the various steel samples. Surfaces imaged two months after coating deposition are labeled (2mo). (b) Complex that EDTA forms around metal cations such as Fe^{2+}. (c) Schematic of rust formation due to the acidic environment caused by the silica layer and PDMS grafting process.

before the solution gelled. Neutralizing the solution caused gelation within seconds. Following this adjustment to pH 5.5, no visible corrosion was detected on the sample coated solely with the silica layer, likely because the number of Cl^- ions in the solution was reduced by four orders of magnitude (depicted in step 3 of Fig. 1). However, upon grafting the PDMS chains to this pH-corrected silica layer, corrosion was again optically apparent immediately following the PDMS deposition (Fig. 2(a)). This surface corrosion was the result of the HCl formed from the hydrolysis of the chlorosilane precursor, as shown in step 5/6 of Fig. 1.

To prevent the HCl from corroding the steel surface, ethylenediamine tetraacetic acid (EDTA) was introduced as a chelating agent in the coating solution. EDTA forms complexes with metal ions in a consistent 1 : 1 ratio, irrespective of the ion's charge. This ligand's ability to create stable complexes can be traced back to its multi-dentate nature, which encapsulates a metal cation in a cage-like structure (Fig. 2(b)). This encapsulation effectively prevents cations from potential interactions with other molecules, such as Cl^- ions.[34] To disperse the EDTA, it was dissolved in a phosphate buffer solution with a pH of 6.5 before mixing with the silica solution (non-pH corrected) in a 1 : 1 weight ratio. This mixture both utilized EDTA's chelating properties and also reduced the acidity of the silica solution, similar to the pH correction performed above. Additional corrosion was not visually observable on this coated steel sample, both immediately after coating as well as two months later (bottom right, Fig. 2(a)). Note that the stains visible in the bottom right image of Fig. 2(a) were present prior to coating the surface. A control experiment was also conducted, where the 1 : 1 phosphate buffer solution was mixed with the non-pH corrected silica solution and applied to the steel (*i.e.*, the same formulation as above but without EDTA). Similar to the pH-corrected silica results, corrosion was not visually detected when this silica solution alone was deposited, but it was readily visible following PDMS deposition. Accordingly, the lack of visible corrosion observed with the silica containing EDTA can indeed be attributed to the EDTA and not the use of the phosphate buffer.

Fig. 3 presents SEM and EDS analyses, highlighting the microstructural and elemental characteristics of (a) bare carbon steel, (b) silica/EDTA/PDMS-coated steel, and (c) corroded silica/EDTA/PDMS-coated steel imaged after 1.5 years. SEM imaging confirmed the formation of a uniform, crack-free silica/EDTA/PDMS coating over the carbon steel substrate (Fig. 3(b)), with a thickness of 280 ± 100 nm as measured by optical profilometry (Methods). EDS analysis of the coated surface identified Si and O as the dominant elements in the coating, while Fe signals originating from the underlying substrate were also observed. Steel coated with silica made from TEOS without EDTA or the buffer solution demonstrated a greater thickness of 460 ± 60 nm. The higher concentration of the precursor solution resulted in a silica layer ~60% thicker than the silica/EDTA/PDMS coating.

For the silica/EDTA/PDMS-coated steel imaged 1.5 years after coating deposition, SEM analysis revealed extensive corrosion across the majority of the surface (Fig. 3(c)). EDS analysis of the corrosion products predominantly identified Fe and O, with no detectable Si, indicating complete degradation of the protective coating in these regions. Conversely, in intact, non-corroded areas, the presence of Si and O confirmed the partial retention of the coating on the substrate. Note that these samples were those exposed to the electrochemical characterization (discussed below), and further experiments would be necessary to assess performance in an actual service environment.

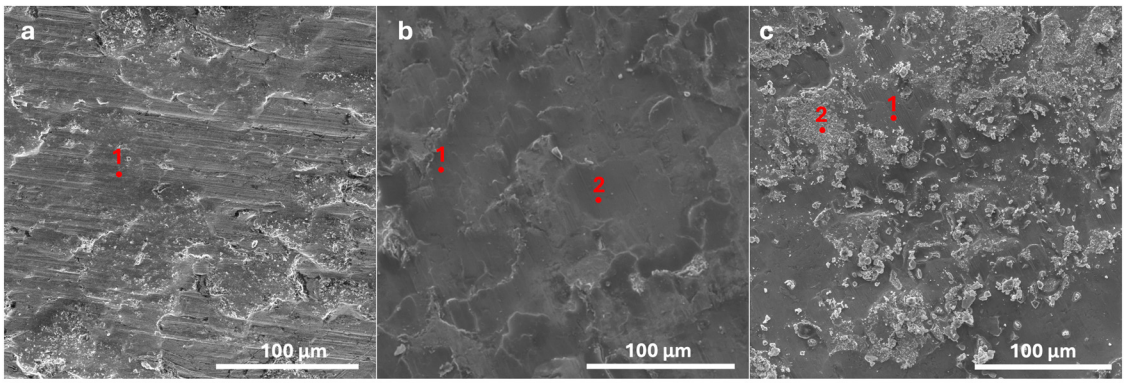

1			
Element	Weight %	Atomic %	Error %
FeL	100.00	100.00	4.10

1			
Element	Weight %	Atomic %	Error %
O K	24.76	47.67	6.89
FeL	55.39	30.55	6.21
SiK	19.85	21.78	6.59
2			
O K	19.26	41.43	7.53
FeL	66.30	40.87	5.49
SiK	14.44	17.70	7.52

1			
Element	Weight %	Atomic %	Error %
O K	23.04	46.34	7.10
FeL	60.62	34.93	6.00
SiK	16.34	18.72	6.91
2			
O K	31.65	61.78	6.79
FeL	68.35	38.22	6.77

Fig. 3 SEM images and EDS analyses of (a) bare carbon steel, (b) silica/EDTA/PDMS-coated carbon steel, and (c) corroded silica/EDTA/PDMS-coated carbon steel imaged 1.5 years after coating deposition. Numbered spots show areas where EDS data were collected, with results displayed in the tables below each corresponding image.

The surface metrology of the coated samples was further investigated. Representative magnified images of the surfaces are shown in Fig. 4, and their roughness values (root-mean-squared surface roughness, S_q, and maximum surface valley depth, S_v) are plotted in Fig. 5. Several points are worthy of discussion. First, localized corrosion spots were readily observable on the bare metal surface. This may be attributed to the sample preparation administered, where the steel substrates were only rinsed with isopropyl alcohol prior to coating deposition. This rinse, while beneficial for cleaning, did not eliminate pre-existing corrosion on the surface that could be removed by polishing. However, this small amount of initial corrosion is more realistic of an actual use case for steel, which can be exposed to the environment for days or even years prior to use or coating deposition.

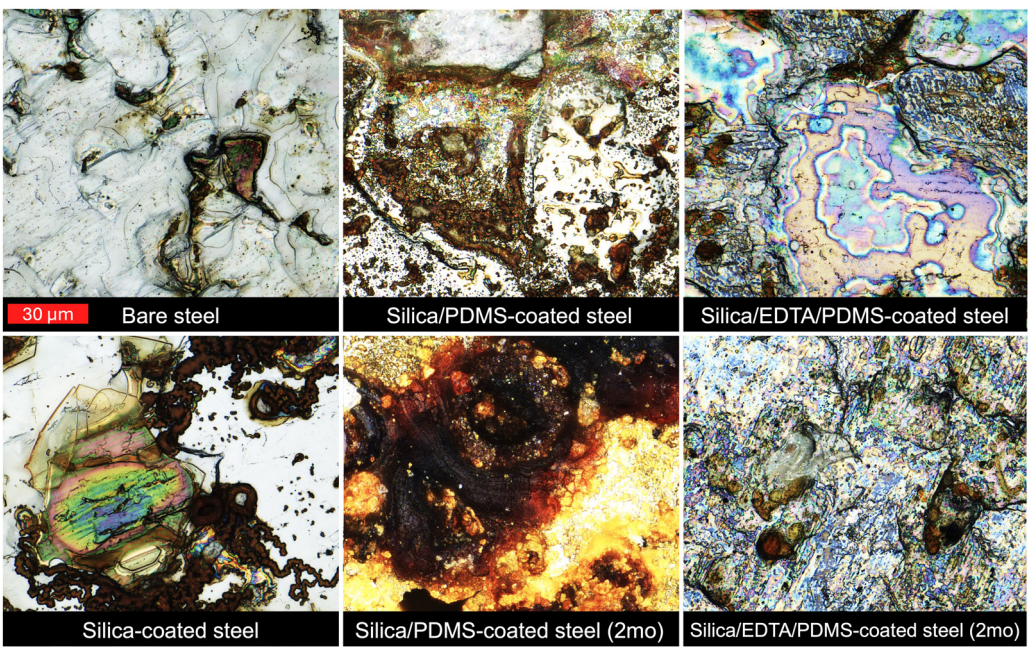

Fig. 4 Microscope images of the various surfaces. ''2mo'' denotes surfaces imaged two months after coating deposition. The 'rainbows' are caused by the optical interference of the thin silica film, though macroscopically the surface was transparent to the naked eye.

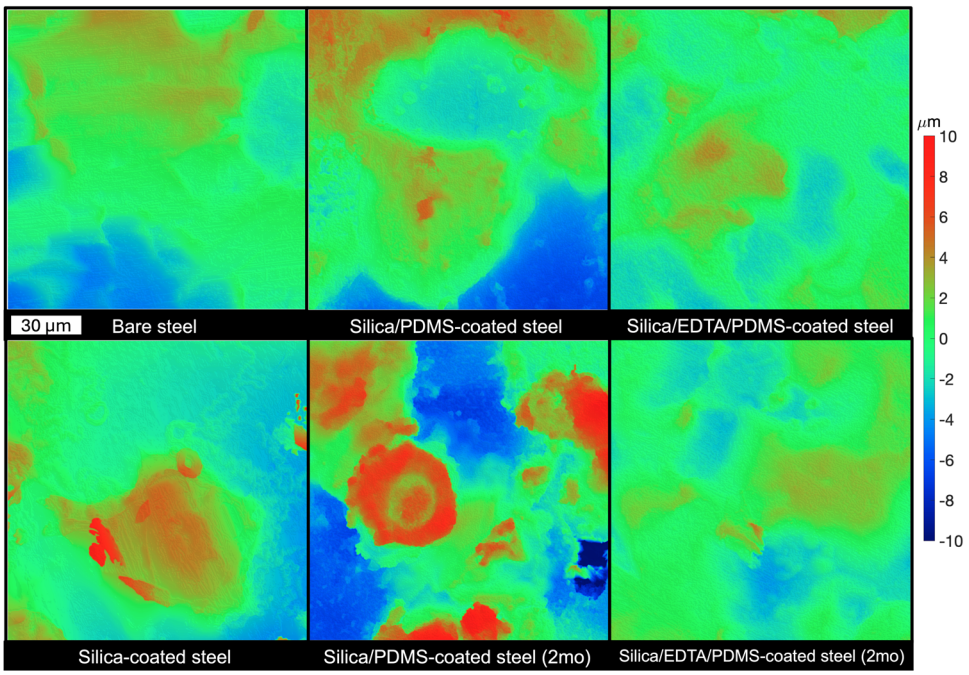

Fig. 5 Heightmaps of the six different surfaces investigated in this study. "2mo" denotes surfaces imaged two months after coating deposition.

Second, after depositing and curing the silica layer without EDTA, the presence of corrosion sites increased, which again was optically apparent on a macroscopic scale (Fig. 2(a)). The addition of the grafted PDMS further increased the visible corrosion on the surface, and re-imaging the surface after two months allowed the corrosion to propagate substantially across the entire substrate. Pronounced irregularities, resembling deep valleys on the steel surface, were observed after this two-month incubation time.

In contrast, the sample coated with the silica/EDTA solution prior to grafting the omniphobic PDMS displayed remarkably little additional corrosion. After the same two-month period, the sample's appearance remained largely unchanged with no significant color deviation. While there were minor corroded areas, the amount present was consistent with the steel surface prior to coating deposition, indicating that no additional corrosion was caused, at least visually, by the silica or omniphobic PDMS. Note that many corrosion environments require mitigation solutions lasting years if not decades, and so extended studies would be needed to confirm the long-term anti-corrosion performance of the silica/EDTA grafted with the omniphobic PDMS. However, as the main objective of this work was to prevent the corrosion caused by the omniphobic formulation during deposition (due to the presence of HCl), assessing the coated steel's performance after two months was sufficient in this regard. The images shown in Fig. 3(c) do, however, suggest that certain electrochemical environments are indeed able to corrode the coated steel substrate after 18 months of incubation time.

Surface corrosion was also identifiable from the surface roughness parameters of the different samples. Representative heightmaps of the various surfaces are shown in Fig. 5, and their metrology parameters are plotted in Fig. 6(a) and (b). Root-mean-squared surface roughness (S_q) was measured to determine the overall average roughness of the surfaces, and the maximum valley depth (S_v) was measured as corrosion is a

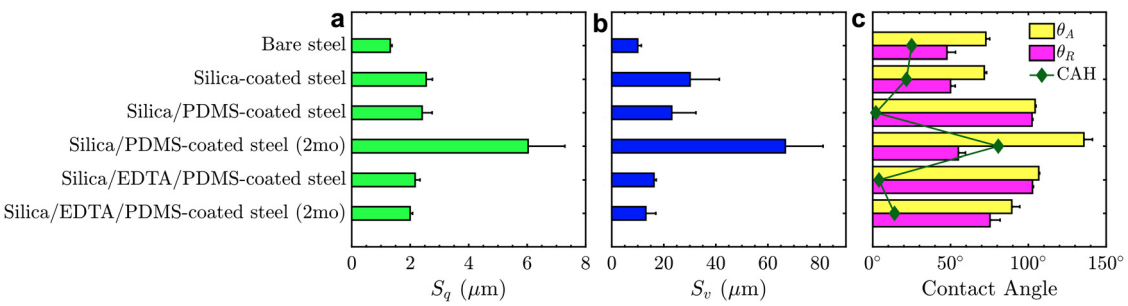

Fig. 6 3D laser scanning microscope measurements of (a) S_q (root-mean-squared roughness) and (b) S_v (maximum valley depth) of the bare and coated steel surfaces. (c) Advancing water contact angle, receding water contact angle, and contact angle hysteresis of the same surfaces.

subtractive process and would therefore increase as the steel corroded away. While the addition of the silica layer appeared to increase the roughness of the steel surface from S_q = 1.3 ± 0.1 μm to 2.5 ± 0.2 μm (Fig. 6(a)), this was actually an artifact of the optical metrological assessment of the thin, conformal transparent film covering the steel. For example, a zoomed-in assessment of the silica surface exhibited a surface roughness of S_q = 80 ± 50 nm, with some spots as smooth as S_q = 27 nm. Overall, the roughness of the steel remained around 1–2.5 μm for all surfaces except the highly corroded silica/PDMS surface without EDTA that had aged for two months, which exhibited S_q = 6 ± 1 μm.

The maximum valley depth data was more revealing (Fig. 6(b)). Initially the bare steel exhibited valleys with depths around S_v = 10 μm. The addition of the silica layer, with or without the PDMS, increased this to ∼30 μm, and after two months this further increased to 67 μm. With the addition of EDTA into the silica formulation, even after two months, the valleys were only S_v = 13 ± 4 μm deep, statistically equivalent to the bare steel using a student's *t*-test (*p*-value: 0.7).

The wetting behavior of the various surfaces with water was also examined (Fig. 6(c)). Unsurprisingly, both the bare steel and steel coated with the silica layer were hydrophilic and exhibited a contact angle hysteresis (CAH) > 20°. Conversely, steel coated with either the silica/PDMS or EDTA/silica/PDMS exhibited advancing and receding water contact angles around θ_A = 106° and θ_R = 103°, and a resultant CAH around 3°–4°. Because the wettability of these surfaces was determined by the PDMS layer, the corrosion observed at the metal/silica interface for the silica/PDMS-coated samples (Fig. 2–4) did not affect the omniphobicity of the coated surface. Note that only water contact angles were measured here, but identical water contact angles for PDMS grafted to silica have been observed for omniphobic PDMS.[9]

The potentiodynamic polarization technique was employed to investigate the corrosion resistance of the various samples and their corresponding polarization curves are shown in Fig. 7(a). Alongside this, LPR was measured at 10-minute intervals and their polarization resistances over time are shown in Fig. 7(b). The bare steel exhibited a current density of 2×10^{-4} A cm^{-2}, and this was slightly lower than the steel coated only with silica (6×10^{-4} A cm^{-2}). These findings indicate that the silica layer itself did not provide any corrosion resistance.

In contrast, the corrosion current density was two orders of magnitude smaller for the EDTA/silica/PDMS-coated steel (∼10^{-6} A cm^{-2}), and this was roughly equivalent to the steel coated with the silica/PDMS without the addition of EDTA. Moreover, there was a noticeable decrease in the anodic slope for both PDMS-coated samples compared to bare metal and the silica-coated steel, suggesting the existence of a passivating layer that prevented metal interactions with the environment. This passivating layer, which stabilizes the current density even at high potential, is likely due to the omniphobic PDMS layer which limits ion diffusion from the solution to the underlying substrate. This observation suggests that the omniphobic PDMS layer, in the absence of EDTA and with some initial corrosion present, still functions as an effective barrier, amplifying the system's corrosion resistance. Nevertheless, the precise impact of the addition of EDTA into the silica layer on the metal's corrosion dynamics remains unknown based solely on the polarization curve. It should be noted that while fewer areas of visible rust were observed for the bare steel and silica-coated steel, their exposure to the electrolyte solution during the potentiodynamic polarization measurement resulted in visible rust on their surface. This was not observed for the PDMS-containing samples, which corroborates the significant current density differences shown in Fig. 7(a).

Furthermore, the LPR results in Fig. 7(b) indicate a higher polarization resistance (indicative of decreased current density and better corrosion behavior) for all coated samples (∼16–18 kΩ cm^2 at 90 min) compared to bare metal (∼2.5 kΩ cm^2 at 90 min), regardless of the presence of EDTA, corroborating the findings from the polarization curves. Notably, the silica/EDTA/PDMS samples aged for 2 months exhibited an even greater polarization resistance (∼40 kΩ cm^2 at 90 min) than the same surface evaluated a few days after coating deposition. To better understand these observations, EIS tests were conducted.

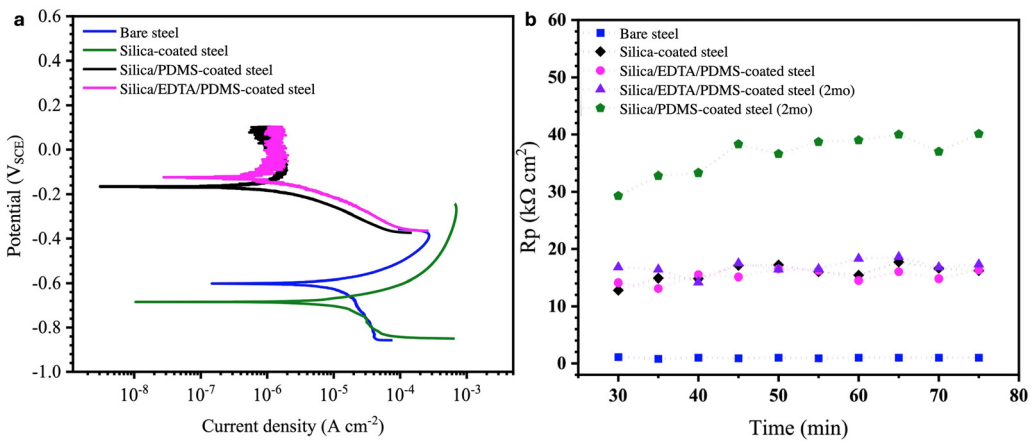

Fig. 7 (a) Potentiodynamic polarization data for different samples, and (b) corresponding LPR results including surfaces aged for two months, denoted by (2mo).

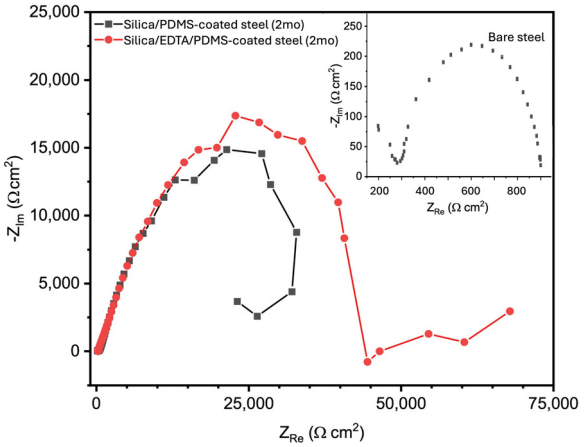

Fig. 8 Nyquist plot comparing aged-coated samples and bare metal, where the *x*-axis represents the real part of the impedance, and the *y*-axis shows the imaginary part of the impedance, capturing resistive and capacitive/inductive behaviors, respectively.

When evaluated in a borate buffer solution (pH 6.0), the Nyquist plot for bare carbon steel exhibited a singular capacitive loop with a polarization resistance measured to be $\sim$1000 Ω cm^2. This comparatively low polarization resistance value relative to the coated samples is indicative of the active corrosion process on the unprotected steel substrate.[35] In contrast, samples coated with silica/PDMS exhibited a marked enhancement in their polarization resistance, $\sim$30 000 Ω cm^2. An inductive loop was also present at lower frequencies (*i.e.* higher Z_{Re} values in Fig. 8), indicative of a continuing corrosion process, though at a slow rate. This inductive loop can be attributed to a sequential mechanism, characterized by the adsorption and subsequent relaxation of intermediates, predominantly FeOH species. The magnitude of this loop directly correlates with the FeOH adsorption-relaxation rate.[36,37] The silica/PDMS-coated sample, left untouched for two months in the laboratory environment and exposed to ambient air, mirrored this behavior, and this was not surprising given the visibly corroded surface evident in Fig. 2–4.

Incorporating the chelating agent within the silica layer enhanced the coating's corrosion resistance, evidenced by a substantial increase in polarization resistance to 40 000 Ω cm^2, consistent with LPR data in Fig. 7(b). Even after two months of being left in the laboratory exposed to air, the silica/EDTA/PDMS sample still showed no signs of an inductive loop (*i.e.* no continued corrosion process) unlike the coated surface lacking EDTA. It is theorized that EDTA's capability to form chelates with Fe^{2+} and Fe^{3+} ions may prohibit the adsorption and relaxation of FeOH.[33] This effectively disrupts the charge transfer processes integral to corrosion. Such interference not only suppresses the appearance of the inductive loop but also boosts the steel's overall resistance to corrosion, as reflected by the higher polarization resistance values.

After the EIS and potentiodynamic polarization tests, water contact angles of the samples aged for 2 months were reassessed to understand their wetting behavior following solution exposure and potential corrosion (Fig. 6(c)). Both advancing and receding contact angles of the silica/EDTA/PDMS-coated surfaces decreased to below 90°, and the CAH increased to $\sim$15°. This degradation in the omniphobic properties potentially stemmed from a partial removal of the PDMS chains due to the applied potential. However, these slightly altered angles were substantially greater than those observed for the bare steel or silica-coated steel, indicating that the majority of the PDMS still remained on the surface. Moreover, the corrosion experienced did not significantly increase the surface roughness (Fig. 6(a) and (b)) which would magnify the measured contact angles. Conversely, the silica/PDMS-coated steel fabricated without the addition of EDTA was substantially rougher, with deeper valleys, and more pronounced peaks due to corrosion, as shown above in Fig. 7. This altered topography caused water droplets to pin on these texture elements, leading to a substantially larger CAH of $\sim$80°.

Summary and conclusion

The primary objective of this study was to formulate an omniphobic coating tailored for low carbon steel surfaces and to understand the anti-corrosion behavior of the coating. To achieve this, a silica layer was first deposited onto the metal surface, which contained EDTA diluted using a phosphate buffer. PDMS was grafted to the surface of this silica layer using vapor-phase chlorosilane deposition, resulting in an omniphobic surface exhibiting low contact angle hysteresis with fluid droplets. Not only did the phosphate buffer partially neutralize the acidic silica solution, the EDTA chelating agent prevented the incipience of corrosion caused by the silica and PDMS deposition, both of which contain hydrochloric acid.

The findings presented here indicate that the omniphobic PDMS layer acts as a corrosion barrier, constraining ion mobility from the solution to the substrate, thereby reducing corrosion rates. However, the HCl trapped during the silica and PDMS deposition eventually permeates to the steel, inducing corrosion underneath the coating. This corrosion fosters deeper valleys and amplified surface roughness, increasing the contact angle hysteresis and, consequently, diminishing the surface's omniphobic properties. A full layer of rust was visually apparent on the surface of the steel coated with the silica/PDMS layer.

Conversely, incorporating EDTA into a buffer solution during the silica layer's application resulted in a coating that reduced corrosion in three ways. First, the presence of the omniphobic PDMS reduced ion transfer by preventing water ingress. Second, the buffer solution neutralized the majority of the HCl present in the silica formulation prior to coating deposition. Finally, EDTA embedded within the silica layer prevented the propagation of corrosion by encapsulating metal cations. The net result of these three coating features was a thin omniphobic layer that remained visually uncorroded even after applying a polarization potential. Supporting this, roughness parameters remained consistent two months after evaluating

the electrochemical properties of the coated steel, and these were corroborated by optical observations. Furthermore, EIS data revealed the chelating agent's presence eliminated the inductive loop (indicative of continued corrosion) that was observed in samples not containing EDTA, while simultaneously boosting resistance to levels more than 40 times that of the bare metal. While the CAH of the optimal coated sample did increase following all the testing and after two months of aging at ambient conditions, it remains to be determined if the slight degradation in omniphobicity was due to the initial corrosion present on the unpolished steel, scission along the backbone of the PDMS chains, or partial delamination of the silica layer. Regardless, the coating developed here can provide omniphobic and anti-corrosion properties to metallic substrates that would be severely corroded by conventional omniphobic coating fabrication techniques, for applications ranging from the protection of instrumentation in factories, to oil and gas pipelines, to marine vessels and off-shore infrastructure, to agricultural vehicles and machinery.

Data availability

Data for this article, including the raw data for Fig. 5–8, are available on Figshare at **https://doi.org/10.6084/m9.figshare.28760897**.

Conflicts of interest

There are no conflicts to declare.

Acknowledgements

The authors acknowledge that this work was conducted at the University of Toronto, on the traditional lands of the Huron-Wendat, the Seneca and the Mississauga of the Credit. This project was supported by the Canada Foundation for Innovation, through grant no. 41543 and 43719, and the Natural Sciences & Engineering Research Council, through grants RGPIN-2018-04272 and RGPIN-2023-04641.

References

1 E. Ozkan, A. Mondal, M. Douglass, S. P. Hopkins, M. Garren, R. Devine, R. Pandey, J. Manuel, P. Singha, J. Warnock and H. Handa, Bioinspired Ultra-Low Fouling Coatings on Medical Devices to Prevent Device-Associated Infections and Thrombosis, *J. Colloid Interface Sci.*, 2022, **608**, 1015–1024, DOI: **10.1016/j.jcis.2021.09.183**.

2 Y. Zhu, G. McHale, J. Dawson, S. Armstrong, G. Wells, R. Han, H. Liu, W. Vollmer, P. Stoodley, N. Jakubovics and J. Chen, Slippery Liquid-Like Solid Surfaces with Promising Antibiofilm Performance under Both Static and Flow Conditions, *ACS Appl. Mater. Interfaces*, 2022, **14**(5), 6307–6319, DOI: **10.1021/acsami.1c14533**.

3 T. R. Roberts, D. C. Leslie, A. P. Cap, L. C. Cancio and A. I. Batchinsky, Tethered-Liquid Omniphobic Surface Coating Reduces Surface Thrombogenicity, Delays Clot Formation and Decreases Clot Strength Ex Vivo, *J. Biomed. Mater. Res., Part B*, 2020, **108**(2), 496–502, DOI: **10.1002/jbm.b.34406**.

4 C. Yang, Q. Wu, L. Zhong, C. Lyu, G. He, C. Yang, X. Li, X. Huang, N. Hu, M. Chen, T. Hang and X. Xie, Liquid-like Polymer-Based Self-Cleaning Coating for Effective Prevention of Liquid Foods Contaminations, *J. Colloid Interface Sci.*, 2021, **589**, 327–335, DOI: **10.1016/j.jcis.2021.01.014**.

5 C. A. Robbins, Y. Yin, A. J. Hanson, J. Blotevogel, T. Borch and T. Tong, Mitigating Membrane Wetting in the Treatment of Unconventional Oil and Gas Wastewater by Membrane Distillation: A Comparison of Pretreatment with Omniphobic Membrane, *J. Membr. Sci.*, 2022, **645**, 120198, DOI: **10.1016/j.memsci.2021.120198**.

6 J. Li, S. Guo, Z. Xu, J. Li, Z. Pan, Z. Du and F. Cheng, Preparation of Omniphobic PVDF Membranes with Silica Nanoparticles for Treating Coking Wastewater Using Direct Contact Membrane Distillation: Electrostatic Adsorption vs. Chemical Bonding, *J. Membr. Sci.*, 2019, **574**, 349–357, DOI: **10.1016/j.memsci.2018.12.079**.

7 X. Zhao, M. A. R. Khandoker and K. Golovin, Non-Fluorinated Omniphobic Paper with Ultralow Contact Angle Hysteresis, *ACS Appl. Mater. Interfaces*, 2020, **12**(13), 15748–15756, DOI: **10.1021/acsami.0c01678**.

8 X. Zhao, B. Khatir, K. Mirshahidi, K. Yu, J. N. Kizhakkedathu and K. Golovin, Macroscopic Evidence of the Liquidlike Nature of Nanoscale Polydimethylsiloxane Brushes, *ACS Nano*, 2021, **15**(8), 13559–13567, DOI: **10.1021/acsnano.1c04386**.

9 B. Khatir, S. Shabanian and K. Golovin, Design and High-Resolution Characterization of Silicon Wafer-like Omniphobic Liquid Layers Applicable to Any Substrate, *ACS Appl. Mater. Interfaces*, 2020, **12**(28), 31933–31939, DOI: **10.1021/acsami.0c06433**.

10 L. Wang and T. J. McCarthy, Covalently Attached Liquids: Instant Omniphobic Surfaces with Unprecedented Repellency, *Angew. Chem., Int. Ed.*, 2016, **55**(1), 244–248, DOI: **10.1002/anie.201509385**.

11 B. Khatir, Z. Azimi Dijvejin, P. Serles, T. Filleter and K. Golovin, Molecularly Capped Omniphobic Polydimethylsiloxane Brushes with Ultra-Fast Contact Line Dynamics, *Small*, 2023, 2301142, DOI: **10.1002/smll.202301142**.

12 J. Liu, Y. Sun, X. Zhou, X. Li, M. Kappl, W. Steffen and H. Butt, One-Step Synthesis of a Durable and Liquid-Repellent Poly (Dimethylsiloxane) Coating, *Adv. Mater.*, 2021, 2100237.

13 L. Zhang, Z. Guo, J. Sarma, W. Zhao and X. Dai, Gradient Quasi-Liquid Surface Enabled Self-Propulsion of Highly Wetting Liquids, *Adv. Funct. Mater.*, 2021, **31**(13), 2008614, DOI: **10.1002/adfm.202008614**.

14 E. Kayahan, H. Oktem, F. Hacizade, H. Nasibov and O. Gundogdu, Measurement of Surface Roughness of Metals Using Binary Speckle Image Analysis, *Tribol. Int.*, 2010, **43**(1), 307–311, DOI: **10.1016/j.triboint.2009.06.010**.

15 E. Wierzbicka, B. Vaghefinazari, S. V. Lamaka, M. L. Zheludkevich, M. Mohedano, L. Moreno, P. Visser, A. Rodriguez, J. Velasco, R. Arrabal and E. Matykina, Flash-PEO as an Alternative to Chromate Conversion Coatings for Corrosion Protection of Mg Alloy, *Corros. Sci.*, 2021, **180**, 109189, DOI: 10.1016/j.corsci.2020.109189.

16 N. Ghavidel, S. R. Allahkaram, R. Naderi, M. Barzegar and H. Bakhshandeh, Corrosion and Wear Behavior of an Electroless Ni-P/Nano-SiC Coating on AZ31 Mg Alloy Obtained through Environmentally-Friendly Conversion Coating, *Surf. Coatings Technol.*, 2020, **382**, 125156, DOI: 10.1016/j.surfcoat.2019.125156.

17 M. A. Hafeez, A. Farooq, A. Zang, A. Saleem and K. M. Deen, Phosphate Chemical Conversion Coatings for Magnesium Alloys: A Review, *J. Coatings Technol. Res.*, 2020, **17**(4), 827–849, DOI: 10.1007/s11998-020-00335-2.

18 C. Wang, W. Gao, N. Liu, Y. Xin, X. Liu, X. Wang, Y. Tian, X. Chen and B. Hou, Covalent Organic Framework Decorated TiO_2 Nanotube Arrays for Photoelectrochemical Cathodic Protection of Steel, *Corros. Sci.*, 2020, **176**, 108920, DOI: 10.1016/j.corsci.2020.108920.

19 F. Xie, J. Li, T. Zou, D. Wang, M. Wu and X. Sun, Stress Corrosion Cracking Behavior Induced by Sulfate-Reducing Bacteria and Cathodic Protection on X80 Pipeline Steel, *Constr. Build. Mater.*, 2021, **308**, 125093, DOI: 10.1016/j.conbuildmat.2021.125093.

20 M. D. Silva Campos, C. Blawert, N. Scharnagl, M. Störmer and M. L. Zheludkevich, Cathodic Protection of Mild Steel Using Aluminium-Based Alloys, *Materials*, 2022, **15**, 1301, DOI: 10.3390/ma15041301.

21 X. Cheng, J. Xia, R. Wu, W. Jin and C. Pan, Optimisation of Sacrificial Anode Cathodic Protection System in Chloride-Contaminated Reinforced Concrete Structure, *J. Build. Eng.*, 2022, **45**, 103515, DOI: 10.1016/j.jobe.2021.103515.

22 D. Thomas, R. R, E. Philip, R. Sindhu, S. B. Ulaeto, A. Pugazhendhi and M. K. Awasthi, Developments in Smart Organic Coatings for Anticorrosion Applications: A Review, *Biomass Convers. Biorefin.*, 2022, **12**(10), 4683–4699, DOI: 10.1007/s13399-022-02363-x.

23 M. Drozda and A. Miszczyk, Selection of Organic Coating Systems for Corrosion Protection of Industrial Equipment, *Coatings*, 2022, **12**, 523, DOI: 10.3390/coatings12040523.

24 M. S. Nunes, R. M. Bandeira, F. C. Figueiredo, J. R. dos Santos Junior and J. M. E. de Matos, Corrosion Protection of Stainless Steel by a New and Low-Cost Organic Coating Obtained from Cashew Nutshell Liquid, *J. Appl. Polym. Sci.*, 2023, **140**(5), e53420, DOI: 10.1002/app.53420.

25 Y. Ye, D. Yang, D. Zhang, H. Chen, H. Zhao, X. Li and L. Wang, POSS-Tetraaniline Modified Graphene for Active Corrosion Protection of Epoxy-Based Organic Coating, *Chem. Eng. J.*, 2020, **383**, 123160, DOI: 10.1016/j.cej.2019.123160.

26 M. Honarvar Nazari, Y. Zhang, A. Mahmoodi, G. Xu, J. Yu, J. Wu and X. Shi, Nanocomposite Organic Coatings for Corrosion Protection of Metals: A Review of Recent Advances, *Prog. Org. Coat.*, 2022, **162**, 106573, DOI: 10.1016/j.porgcoat.2021.106573.

27 M. Izadi, T. Shahrabi, I. Mohammadi, B. Ramezanzadeh and A. Fateh, The Electrochemical Behavior of Nanocomposite Organic Coating Based on Clay Nanotubes Filled with Green Corrosion Inhibitor through a Vacuum-Assisted Procedure, *Composites, Part B*, 2019, **171**, 96–110, DOI: 10.1016/j.compositesb.2019.04.019.

28 X. Gao, R. Yan, Y. Lv, H. Ma and H. Ma, In Situ Pretreatment and Self-Healing Smart Anti-Corrosion Coating Prepared through Eco-Friendly Water-Base Epoxy Resin Combined with Non-Toxic Chelating Agents Decorated Biomass Porous Carbon, *J. Cleaner Prod.*, 2020, **266**, 121920, DOI: 10.1016/j.jclepro.2020.121920.

29 T. Almubarak, J. H. Ng, R. Ramanathan and H. A. Nasr-El-Din, From Initial Treatment Design to Final Disposal of Chelating Agents: A Review of Corrosion and Degradation Mechanisms, *RSC Adv.*, 2022, **12**(3), 1813–1833, DOI: 10.1039/D1RA07272B.

30 Y. Shi, L. Yu, S. Chen, Y. He, X. Yang, L. Duan and J. Cai, Effects of L-Glutamic Acid, N, N-Diacetic Acid as Chelating Agent on Acidification of Carbonate Reservoirs in Acidic Environments, *J. Nat. Gas Sci. Eng.*, 2020, **82**, 103494, DOI: 10.1016/j.jngse.2020.103494.

31 F. Bosaid, H. Aksel, S. Makowka and A. A. Azim, Surface and Structural Changes in Root Dentine by Various Chelating Solutions Used in Regenerative Endodontics, *Int. Endod. J.*, 2020, **53**(10), 1438–1445, DOI: 10.1111/iej.13354.

32 Y. C. Shinta, B. Zaman and S. Sumiyati, Citric Acid and EDTA as Chelating Agents in Phytoremediation of Heavy Metal in Polluted Soil: A Review, *IOP Conf. Ser. Earth Environ. Sci.*, 2021, **896**(1), 12023, DOI: 10.1088/1755-1315/896/1/012023.

33 K. Zhang, Z. Dai, W. Zhang, Q. Gao, Y. Dai, F. Xia and X. Zhang, EDTA-Based Adsorbents for the Removal of Metal Ions in Wastewater, *Coord. Chem. Rev.*, 2021, **434**, 213809, DOI: 10.1016/j.ccr.2021.213809.

34 M. A. Zaitoun and C. T. Lin, Chelating Behavior between Metal Ions and EDTA in Sol−Gel Matrix, *J. Phys. Chem. B*, 1997, **101**(10), 1857–1860, DOI: 10.1021/jp963102d.

35 J. Chen, X. Wang, H. Ma, Z. Huo and Y. Wang, Experimental Investigation on Corrosion Behavior of X80 Pipeline Steel under Carbon Dioxide Aqueous Conditions, *ACS Omega*, 2022, **7**(7), 6142–6150, DOI: 10.1021/acsomega.1c06613.

36 J. O. Bockris, D. Drazic and A. R. Despic, The Electrode Kinetics of the Deposition and Dissolution of Iron, *Electrochim. Acta*, 1961, **4**(2), 325–361, DOI: 10.1016/0013-4686(61)80026-1.

37 V. S. Sastri and S. Vedula, Green Corrosion Inhibitors: Theory and Practice, *Wiley series in corrosion*, Wiley, Hoboken, N.J., 1st edn, 2011.

